HHS Public Access

Author manuscript

Nat Plants. Author manuscript; available in PMC 2019 July 21.

Published in final edited form as:

Nat Plants. 2019 February ; 5(2): 212–224. doi:10.1038/s41477-018-0348-x.

Noncanonical ATG8-ABS3 interaction controls senescence in plants

Min Jia[1,3], **Xiayan Liu**[1,3], **Hui Xue**[1], **Yue Wu**[2], **Lin Shi**[2], **Rui Wang**[1,4], **Yu Chen**[1], **Ni Xu**[1], **Jun Zhao**[1], **Jingxia Shao**[1], **Yafei Qi**[1], **Lijun An**[1], **Jen Sheen**[2], and **Fei Yu**[1,*]

[1]State Key Laboratory of Crop Stress Biology for Arid Areas and College of Life Sciences, Northwest A&F University, Yangling, Shaanxi 712100, People's Republic of China

[2]Department of Molecular Biology and Centre for Computational and Integrative Biology, Massachusetts General Hospital, and Department of Genetics, Harvard Medical School, Boston, Massachusetts 02114, USA

[3]These authors contributed equally to this work.

[4]Present address: Department of Molecular Genetics and Center for Applied Plant Science, Ohio State University, Columbus, OH 43210, USA

Abstract

Protein homeostasis is essential for cellular functions and longevity, and the loss of proteostasis is one of the hallmarks of senescence. Autophagy is an evolutionarily conserved cellular degradation pathway and is critical for the maintenance of proteostasis. Paradoxically, autophagy deficiency leads to accelerated protein loss by unknown mechanisms. We discover that ABS3 subfamily of multidrug and toxic compound extrusion (MATE) transporters promote senescence in natural and carbon-deprivation conditions in *Arabidopsis thaliana*. The senescence-promoting ABS3 pathway functions in parallel with the longevity-promoting autophagy to balance plant senescence and survival. Surprisingly, ABS3 subfamily MATE proteins interact with ATG8 at late endosome to promote senescence and protein degradation without the canonical cleavage and lipidation of ATG8. This non-autophagic ATG8-ABS3 interaction paradigm is likely conserved among dicots and monocots. Our findings uncover a previously unknown non-autophagic function of ATG8 and an unrecognized senescence regulatory pathway controlled by the ATG8-ABS3-mediated proteostasis.

From ancient tonics to modern molecular interventions, the quest for longevity has always been part of human nature. Nutrient availability is closely tied with growth and longevity in

*Correspondence: flyfeiyu@gmail.com. **Materials & Correspondence:** Further information and requests for resources and reagents should be directed to the corresponding author, Fei Yu (flyfeiyu@gmail.com).

Author contributions

X.L., J. Sheen, and F.Y. conceived the study and designed experiments. M.J., H.X, R.W., Y.C., N.X., J.Z., J. Shao, and Y.Q. performed experiments. M.J., X.L., Y.W., L.S., and L.A. analyzed data. M.J., X.L., J. Sheen, and F.Y. wrote the manuscript with contributions from all authors.

Competing interests

The authors declare no competing interests.

many organisms[1]. In higher plants, the manipulations of nutrient availability, such as the deprivation of carbon or nitrogen sources, can also modulate plant senescence[2,3]. In addition, many key regulators of senescence are conserved in plants, suggesting that the regulation of longevity may be conserved in eukaryotic systems[1,4–7]. Consistent with this notion, the over-expressions of *KIN10* and *KIN11*, encoding plant homologs of AMPK, promote plant longevity in Arabidopsis[7].

Despite the tremendous progress in understanding the control of life span and senescence in yeast and model animals, much less is known mechanistically in higher plants. During senescence, nutrients are mobilized and reallocated to the sink organs, especially seeds, to ensure the reproductive success of plants[8–11]. The proper elaboration of plant senescence is modulated by internal developmental and hormonal signals[10,11]. In addition, external environmental conditions including both biotic and abiotic stresses can also trigger premature plant senescence[12,13].

Autophagy is responsible for the delivery of cellular components to the lysosome/vacuole for degradation especially under nutrient limitation as well as other stress conditions, and is essential for cellular proteostasis and longevity[14]. Canonical autophagy pathway, culminated in the formation of phosphatidylethanolamine (PE) conjugated ATG8 and autophagosome, is highly conserved among eukaryotes including higher plants[3,15]. The hallmark phenotype of plant autophagy mutants is paradoxically an accelerated loss of bulk cellular proteins, especially chloroplast proteins which account for about 80% of total leaf nitrogen, during natural or nutrient deprivation induced senescence[2,3,16,17]. This intriguing yet unexplained phenotype of plant *atg* mutants suggests additional catabolic pathway(s) is operating in the absence of autophagy.

Multidrug and toxic compound extrusion (MATE) family transporters are multidrug efflux carriers and are ubiquitously present in prokaryotic and eukaryotic organisms[18]. In bacteria, MATE is involved in the export of a plethora of xenobiotic compounds including antibiotics[18]. In budding yeast, a MATE protein, YHR032W, was shown to mediate longevity, through modulation of *S*-adenosyl-L-methionine (SAM) level and activation of AMPK[19]. In humans, two plasma membrane localized MATEs are responsible for the extrusion of a diverse spectrum of cationic drugs[20]. Surprisingly, MATE transporter family expanded dramatically in higher plants, and at least 56 putative members were identified in Arabidopsis[21]. Plant MATEs have been shown to reside on various cellular membranes including plasma membrane, chloroplast envelope, endosomal membrane, and tonoplast, and are involved in a diverse array of physiological activities[21–32].

We are interested in elucidating the mechanisms of plant senescence. Previously, we showed that ectopic expressions of two Arabidopsis *MATE* genes, *ABS3* and *ABS4*, in the gain-of-function mutants *abs3–1D* and *abs4–1D* lead to sucrose dependent cell elongation defects[30]. We observed empirically that adult *abs3–1D* and *abs4–1D* plants exhibited precocious senescence, and hypothesized that ABS3 and its close homologs may modulate senescence in Arabidopsis. In this study, we established a molecular framework of a previously unknown senescence regulatory pathway mediated by the ABS3 subfamily MATE proteins in higher plants. Interestingly, the ABS3-mediated senescence pathway necessitates the

physical interaction between ABS3 and ATG8 at late endosome (LE), but does not require ATG8-PE conjugation or the ATG5/7-dependent canonical autophagy. Moreover, this senescence pathway controlled by the ATG8-ABS3 interaction is likely conserved among dicots and monocots. Taken together, our findings uncover a novel function of ATG8 distinct from its canonical role in autophagy and also discover an evolutionarily conserved mechanism that controls senescence in higher plants.

Results

ABS3 subfamily MATE transporters promote senescence in Arabidopsis

To screen for new components of plant senescence pathway, we established a robust assay to monitor the senescence process of Arabidopsis seedlings upon carbon deprivation (C-deprivation) (Supplementary Fig. 1a). When light-grown 7-day-old wild type (WT) seedlings were transferred to medium lacking exogenous sugar and placed in the dark, senescence was induced as indicated by the rapid reduction of chlorophyll and the degradation of cellular proteins (Supplementary Fig. 1b–d). Utilizing this assay, we tested the C-deprivation responses of *abs3–1D*, an activation tagged gain-of-function mutant that shows precocious senescence in adult plants[30]. Compared to the WT, *abs3–1D* showed greatly accelerated senescence upon C-deprivation (Fig. 1a). ABS3 belongs to the MATE transporter family (Supplementary Fig. 1e)[21]. Five additional MATE proteins are closely related to ABS3 in the same phylogenetic clade that we designated the ABS3 subfamily (Fig. 1b, Supplementary Fig. 1e). *abs4–1D*, a gain-of-function allele of *ABS4*, also showed accelerated senescence under C-deprivation (Supplementary Fig. 1f)[30]. To test whether ABS3 subfamily MATEs share redundant functions in C-deprivation induced senescence, we examined the responses of individual loss-of-function *mate* mutants. Among six single *mate* mutants, only *abs3–1* and *abs3l2–1* showed slightly delayed senescence while the progression of senescence in other four *mate* mutants was comparable to that of WT (Fig. 1c, Supplementary Fig. 1g). Next, we analyzed C-deprivation induced senescence in higher order *mate* mutants. A trend of increased degree of delayed senescence was observed in double mutant *mated* (*abs3–1 abs4–1*), quadruple mutant *mateq* (*abs3–1 abs4–1 abs3l1–1 abs3l2–1*), and sextuple mutant *mates* (*abs3–1 abs4–1 abs3l1–1 abs3l2–1 abs3l3–1 abs3l4–1*) (Fig. 1d).

Since quadruple mutant *mateq* showed a pronounced delay of senescence, most analyses were performed with *mateq* in this study. We next carried out in-depth characterizations of C-deprivation responses in WT, *abs3–1D*, and *mateq*. Quantitative analyses showed that chlorophyll reduction and total cellular protein reduction on a fresh tissue weight basis were faster in *abs3–1D* than in WT, but were greatly delayed in *mateq* (Fig. 1e). Coomassie Brilliant Blue (CBB) stained protein gel and immunoblotting of rubisco large subunit (RBCL), showed that reductions of bulk cellular protein and RBCL were hastened in *abs3–1D* and were significantly delayed in *mateq* compared to the WT (Fig. 1f). As expected, C-deprivation effectively induced the accumulation of autophagy marker ATG8-PE (Fig. 1f). At the transcript level, the onset of senescence activates senescence associated genes and represses photosynthesis related genes. Compared to the WT, more acute induction of senescence marker genes *SAG12*, *ORE1*, and *SGR1* was observed in *abs3–1D* while in

mateq the inductions were greatly attenuated (Fig. 1g)[33,34]. Similarly, the repression of genes encoding components of photosynthetic electron transport chain (*CAB3* and *PetC*) and a subunit of chloroplast ribosome (*PRPL13*) was stronger in *abs3–1D* but weaker in *mateq* compared to the gene expression in the WT (Fig. 1g). In addition to C-deprivation, ABS3 subfamily MATEs also promote senescence under nitrogen (N)-starvation (Supplemental Fig. 1h), suggesting they may have a broader role in regulating nutrient stress responses.

In plants, natural and stress-induced senescence are overlapping but distinct processes[11,12]. To determine whether ABS3 subfamily MATEs play a role in natural senescence, we monitored the natural senescence process in WT, *abs3–1D*, and *mateq*. At 16-day-old, the first pair of true leaves had comparable levels of total cellular protein in all three genotypes (Fig. 1h, i). However, the first pair of true leaves of 26-day-old *abs3–1D* showed prominent signs of senescence, accompanied by a massive loss of cellular proteins and chlorophyll, while leaf chlorosis and reduction in protein content were milder in *mateq* compared to those in WT (Fig. 1h, i). Importantly, endogenous promoter driven *ABS3-GFP* fusion gene (*pABS3:ABS3-GFP*) was sufficient to complement the delayed senescence phenotype in *mateq* and *mates*, respectively (Fig. 1j). Together, these data demonstrated that *ABS3* subfamily *MATE* genes are positive regulators for both C-deprivation induced and natural developmental senescence.

ABS3 subfamily MATEs control senescence and proteostasis independent of canonical autophagy

The accelerated senescence phenotype of *abs3–1D* and *abs4–1D* under C-deprivation is reminiscent of plant *atg* mutants (Supplementary Fig. 2a)[35–38]. To probe the relationship between ABS3-mediated pathway and autophagy, we first took a genetic approach and generated higher order mutants of *ATG5*/*7* and *ABS3* subfamily *MATE* genes. Remarkably, the senescence phenotype of *atg7–3* under C-deprivation was effectively suppressed in the *mateq atg7–3* quintuple mutant, suggesting a previously unknown role of ABS3 subfamily MATE proteins in regulating senescence in the absence of canonical autophagy (Fig. 2a). Consistently, the *abs3–1D atg7–3* double mutant was extremely sensitive to C-deprivation, showing far more severe chlorosis (Fig. 2a). Analyses of quintuple mutant *mateq atg5–1* and double mutant *abs3–1D atg5–1* corroborated the observations of *mateq atg7–3* and *abs3–1D atg7–3*, respectively (Supplementary Fig. 2b). The reversal of the early senescence phenotypes of *atg7–3* and *atg5–1* by *mateq* is, to our knowledge, the first genetic condition that could bypass the need for autophagy to prevent senescence in plants. These findings suggest that the activities of ABS3 subfamily MATEs act as a molecular switch for senescence program regardless of whether canonical autophagy is functional.

To understand the molecular basis of these genetic interactions, we analyzed the accumulations of ATG8 and ATG8-PE in these mutants. Consistent with the established functions of ATG5 and ATG7, upon C-deprivation, *atg7–3* or *atg5–1* failed to produce ATG8-PE, but accumulated high levels of ATG8 precursors, including a distinct ATG8 form that is not found in WT (Fig. 2b, Supplementary 2c, d). Despite the opposite senescence phenotypes, *mateq atg7–3* and *abs3–1D atg7–3*, showed ATG8 accumulation patterns that

are similar to that of *atg7–3* (Fig. 2b). In addition, regardless of the C-deprivation treatment, the degradation of NBR1, a cargo receptor and also a substrate for selective autophagy[39], was only blocked when *ATG5* or *ATG7* is mutated, but was not affected in either *abs3–1D* or *mateq* (Fig. 2c). These results suggest that the flux of autophagy is uninterrupted in *abs3–1D* or *mateq*. Importantly, introducing *mateq* to the *atg7–3* or *atg5–1* background did markedly slow down the protein loss during C-deprivation (Fig. 2b, Supplementary Fig. 2d). Meanwhile, adding *abs3–1D* mutation to *atg7–3* or *atg5–1* further escalated the rate of protein loss (Fig. 2b, Supplementary Fig. 2c). Together, our genetic, biochemical, and molecular evidence suggest that ABS3 subfamily MATEs controls senescence and proteostasis independent of autophagy.

In Arabidopsis, LE, multivesicular bodies (MVB), and prevacuole (PVC) are indistinguishable endomembrane compartments controlling the selective trafficking of proteins to the vacuole for degradation[40]. Previously, we have shown that ABS3, ABS4, ABS3L1, and ABS3L2 co-localized with a LE protein, SYP21[30]. We next validated whether all six members of the ABS3 subfamily MATEs reside at LE. When co-expressed in Arabidopsis leaf protoplasts, MATE-GFPs largely overlapped with LE marker mScarlet-ARA7 (Fig. 2d, Supplementary Fig. 2e)[41,42]. Furthermore, *in planta* co-localizations of ABS3-GFP and mCherry-ARA7 were observed in root epidermal cells of dual labeling transgenic lines expressing both *p35S:ABS3-GFP* and *pUBQ10:mCherry-ARA7* (Fig. 2e). Next, we treated transgenic plants *p35S:ABS3-GFP* and *pUBQ10:YFP-ARA7* with wortmannin, a PI3K inhibitor known to cause MVB swelling[40]. Both ABS3-GFP and YFP-ARA7 gave ring-like signals upon wortmannin treatment (Supplementary Fig. 2f). The majority of ABS3-GFP signals was found on the periphery of the rings, likely the LE delimiting membrane, and a minor portion of ABS3-GFP signals was also present inside the rings (Supplementary Fig. 2f, g).

Finally, we tested whether proper function of vacuole is required for ABS3-mediated proteostasis. An estimation of vacuolar cathepsin B-like cysteine protease activity by the Magic Red cathepsin B reagent staining suggested that cathepsin B-like protease activity is higher in *abs3–1D* than that in WT or *mateq* (Supplementary Fig. 2h, i). In addition, when WT, *atg7–3, abs3–1D*, and *abs3–1D atg7–3* seedlings were subjected to C-deprivation and treated with E-64d, a vacuolar cysteine protease inhibitor, E-64d effectively impeded the rate of bulk protein reduction in *atg7–3, abs3–1D*, and *abs3–1D atg7–3* seedlings after 3d C-deprivation (Fig. 2f). These findings suggested ABS3-mediated catabolic pathway is at least partially dependent on the proteolytic activity of the vacuole.

ABS3 subfamily MATEs are novel ATG8 interacting partners at LE

The hyperaccumulation of C-deprivation induced ATG8-PE in *abs3–1D* implied a potential functional link between ABS3 and ATG8. To test this hypothesis, we assessed whether ABS3 physically interacts with ATG8. First, partial co-localization was observed in Arabidopsis leaf protoplasts co-expressing mCherry-ABS3 and GFP-ATG8e (Fig. 3a). Next, we probed potential direct interaction between ABS3 and ATG8 by the BiFC assay in protoplasts and the split-ubiquitin assay in yeast[43,44]. In the BiFC assay, co-expressing YN-ABS3 and YC-ATG8e, but not YN-ABS3 and YC vector or YN vector and YC-ATG8e, in

protoplasts reconstituted punctuated YFP signals that localized to mScarlet-ARA7 labeled LEs (Fig. 3b, Supplementary Fig. 3a). In the split-ubiquitin assay, the interaction of ABS3 or ABS4 with ATG8e activated the expression of reporter genes (Fig. 3c, Supplementary Fig. 3b). To expand our findings, we investigated the interactions between the other five members of the ABS3 subfamily and ATG8e with the BiFC assay, and showed that they interact at LEs (Supplementary Fig. 3c). We also confirmed that all nine Arabidopsis ATG8s (ATG8a-ATG8i) could interact with ABS3 subfamily MATEs (Supplementary Fig. 4). Lastly, we carried out pull-down assay using purified recombinant GST-ATG8e. GST-ATG8e, but not GST, was able to pull down ABS3-GFP from membrane fractions of *p35S:ABS3-GFP* transgenic lines (Fig. 3d). Together, our data support a direct physical interaction between ABS3 and ATG8 at LE.

ATG8-ABS3 interaction is uncoupled from ABS3 transporter activity or the autophagic function of ATG8

The unexpected interaction between ABS3 and ATG8 prompted us to test whether ABS3 has acquired additional functions that could be uncoupled from its MATE transporter activity. To test this possibility, we first compared the amino acid sequences of the ABS3 subfamily MATEs with the MATE transporter of hyperthermophilic archaeon *Pyrococcus furiosus* (PfMATE) and an Arabidopsis MATE AtDTX14, whose crystal structures and essential amino acids for transporter activity have been determined[45,46]. We identified Pro 66 in ABS3 as a conserved residue, whose corresponding residues in PfMATE and AtDTX14 (Pro 26 in PfMATE and Pro 36 in AtDTX1) are indispensable for their transporter activity (Fig. 4a). Converting Pro 66 to alanine in ABS3 would produce a presumably transporter dead version of ABS3. Indeed, ABS3^{P66A} failed to complement the *E. coli* transporter mutant *ΔacrB* as expressing ABS3, but not ABS3^{P66A}, conferred resistance to antibiotic norfloxacin in *ΔacrB* background (Fig. 4b). Co-expressions of GFP-ABS3^{P66A} with mCherry-ABS3 or mScarlet-ARA7 showed nicely overlapping signals, suggesting that the P66A mutation does not alter the subcellular localization of ABS3 (Supplementary Fig. 5a). Next, we checked the interactions between YN-ABS3^{P66A} with YC-ATG8e via BiFC assay in protoplasts, and found that P66A mutation did not hamper the efficiency or the localization of the reconstituted YFP signals (Fig. 4c and Supplementary Fig. 5b, f). Moreover, Arabidopsis transgenic lines expressing *p35S:ABS3^{P66A}* not only hastened senescence under C-deprivation but also resembled *abs3–1D* when grown on soil (Fig. 4d, e, Supplementary Fig. 5g). Together these results indicate that the ATG8-ABS3 interaction, as well as the regulation of senescence by ABS3, can be uncoupled from the transporter function of ABS3.

In canonical autophagy, ATG8 is processed by ATG4 at a conserved C-terminal glycine and a ubiquitin-like conjugation system (ATG7 as E1; ATG3 as E2; ATG12-ATG5-ATG16 as E3) facilitates the formation of ATG8-PE moieties[3,15]. However, our genetic evidence suggests that ABS3-mediated senescence pathway does not rely on ATG5 or ATG7, raising the question of whether the ATG8-ABS3 interaction requires the lipidation of ATG8. To test this, we first determined that Gly 118 of Arabidopsis ATG8e is the conserved glycine (Fig. 4f). YFP signals reconstituted by Gly 118 mutated YC-ATG8e^{G118A} and YN-ABS3 were indistinguishable from those produced by WT YC-ATG8e and YN-ABS3 (Fig. 4g, Supplementary Fig. 5c, f), suggesting the formation of ATG8-PE is not necessary for ATG8-

ABS3 interaction at LE. Furthermore, BiFC assays of YC-ATG8e and YN-ABS3 carried out in *atg7–3* and *atg5–1* mutant protoplasts also yielded punctuated signals at LEs despite the blockage of autophagy and ATG8-PE conjugation (Fig. 4h, i, Supplementary Fig. 5d–f). These data suggest ABS3 could recruit unconjugated ATG8 to the LE and also indicate that the ATG8-ABS3 interaction represents a previous unknown non-autophagic function of ATG8.

ATG8-ABS3 interaction is required for ABS3-mediated senescence

Next, we sought to explore the functional consequence of the disruption of ATG8-ABS3 interaction. ATG8 is known to interact with its interactors via the ATG8-interacting motif (AIM)/LC3-interacting region (LIR)[47]. The iLIR program predicts two potential AIMs in ABS3 and these two AIMs appeared to be conserved in the ABS3 subfamily (Fig. 5a, Supplementary Fig. 6a)[48]. We constructed mutant forms of ABS3 harboring mutations disrupting AIM1 ($ABS3^{mAIM1}$: W278A L281A) and AIM2 ($ABS3^{mAIM2}$: W463A L466A), individually and simultaneously ($ABS3^{mAIM1+mAIM2}$). Co-localization analyses indicated that three mutant forms of ABS3 did not affect LE localization (Supplementary Fig. 6b). When individual AIM was disrupted, YN-$ABS3^{mAIM1}$ or YN-$ABS3^{mAIM2}$ could still reconstitute YFP with YC-ATG8e (Fig. 5b, Supplementary Fig. 6c). But quantifications of BiFC assays showed that disruption of single AIM, especially AIM2 significantly reduced the efficiency of ATG8e-ABS3 interaction (Fig. 5b, Supplementary Fig. 5f). When both AIMs were mutated in $ABS3^{mAIM1+mAIM2}$, we observed dramatically diminished interaction signal between YN-$ABS3^{mAIM1+mAIM2}$ and YC-ATG8e (Fig. 5b, Supplementary Fig. 5f), suggesting these two AIMs are critical mediators of the ATG8-ABS3 interaction.

To investigate the cellular function of the ATG8-ABS3 interaction, we examined the trafficking of ABS3-GFP and $ABS3^{mAIM1+mAIM2}$-GFP in protoplasts. WT protoplasts transfected with *ABS3-GFP* were treated with vacuolar protease inhibitor E-64d or mock treated with DMSO and incubated in sugar free buffer in the dark for 12 hrs. In E-64d but not DMSO treated protoplasts, in addition to the endosomal ABS3-GFP puncta present in the cell periphery, we also detected punctuate ABS3-GFP signals in the vacuole (Fig. 5c). The trafficking of ABS3-GFP to vacuole was also observed in *atg7–3* or *atg5–1* backgrounds (Fig. 5c, Supplementary Fig. 6d). These findings suggest under C-deprivation ABS3-GFP is likely delivered to the vacuole for degradation and this process is independent of autophagy. Strikingly, the delivery of ABS3-GFP to the vacuole was abolished when both AIMs are mutated, as $ABS3^{mAIM1+mAIM2}$-GFP maintained a predominantly endosomal distribution in either the WT or the *atg7–3*/*atg5–1* mutant background regardless of the presence or absence of E-64d (Fig. 5c, Supplementary Fig. 6d). These data indicate that the trafficking of ABS3-GFP to the vacuole is dependent on the ATG8-ABS3 interaction but not autophagy.

To determine the trafficking of ABS3-GFP in planta, we tracked changes of ABS3-GFP and $ABS3^{mAIM1+mAIM2}$-GFP signals in Arabidopsis transgenic lines. In root epidermal cells of seedlings kept under light, both ABS3-GFP and $ABS3^{mAIM1+mAIM2}$-GFP showed endosomal localization regardless of whether E-64d was added (Fig. 5d). In addition to the endosomal ABS3-GFP signals, 12 hr C-deprivation led to diffused GFP signals in the

vacuole (Fig. 5d). The addition of E-64d during C-deprivation treatment led to the accumulation of ABS3-GFP puncta in the vacuole, confirming that the delivery of ABS3-GFP to the vacuole likely leads to its degradation. Consistently, immunoblotting analysis of ABS3-GFP showed a substantial increase of free GFP after C-deprivation, and E-64d treatment during C-deprivation increased accumulation of ABS3-GFP with concomitant decrease of free GFP (Supplementary Fig. 6e). Notably, this C-deprivation stimulated trafficking of ABS3-GFP to the vacuole is disabled when AIMs in ABS3 are disrupted as $ABS3^{mAIM1+mAIM2}$-GFP remained mostly endosomal even under C-deprivation and E-64d treatment (Fig. 5d). Together, these data confirm that ATG8-ABS3 interaction is required for the C-deprivation induced vacuolar degradation of ABS3-GFP.

Finally, to uncover the physiological role of the ATG8-ABS3 interaction in planta, we generated Arabidopsis transgenic lines expressing *p35S:ABS3*$^{mAIM1+mAIM2}$. Despite the high levels of *ABS3*$^{mAIM1+mAIM2}$ transcripts, the progression of C-deprivation induced senescence in *p35S:ABS3*$^{mAIM1+mAIM2}$ lines is comparable to that of the WT, in contrast to the accelerated senescence of *abs3–1D* (Fig. 5e, Supplementary Fig. 6f). Consistent with plant phenotypes, overexpression of *ABS3*$^{mAIM1+mAIM2}$ failed to accelerate protein degradation during C-deprivation (Fig. 5f). When grown on soil, *p35S:ABS3*$^{mAIM1+mAIM2}$ lines resembled WT but not *abs3–1D* (Supplementary Fig. 6g). To investigate whether the availability of total cellular ATG8 pool regulates ABS3-mediated senescence, we overexpressed *ATG8e* in the *abs3–1D* background. Interestingly, dramatically increased protein level of ATG8 does not alter the accelerated senescence of *abs3–1D* under C-deprivation nor did it affect the developmental phenotype of soil-grown *abs3–1D* (Fig. 5g, h, Supplementary Fig. 6h), suggesting the amount of ATG8 is not a limiting factor of ABS3-mediated senescence. Together, these findings suggest that the ATG8-ABS3 interaction may generate a signal to promote senescence and protein degradation, and the involvement of ATG8 in ABS3-mediated senescence pathway provide a function that is opposite to the role of autophagy in senescence prevention.

Conservation of ATG8-ABS3 interaction in plant senescence

ATG8 and *MATE* genes are ubiquitously present in higher plants. To test whether the ATG8-ABS3 interaction in dicotyledonous Arabidopsis represent a conserved mechanism in higher plants, we cloned a ABS3 subfamily *MATE* gene and a *ATG8* gene from monocotyledonous wheat (*Triticum aestivum*) and named these two genes *TaABS3* and *TaATG8d*, respectively, based on their phylogenetic relationship with Arabidopsis MATEs and ATG8s (Supplementary Figs. 1e, 7a, b). Co-localization of TaABS3-GFP with mScarlet-ARA7 in Arabidopsis protoplasts indicated that TaABS3 also resides at LE (Fig. 6a). BiFC assay showed that TaABS3 could interact with TaATG8d (Fig. 6b, Supplementary Fig. 7c). Moreover, we observed cross-species interactions between Arabidopsis ABS3 subfamily MATEs and TaATG8d (Supplementary Fig. 7d). Intriguingly, TaABS3 also harbors two putative AIMs at the conserved positions compared to those found in ABS3 (Fig. 6c). Consistent with findings in Arabidopsis, the disruption of both AIMs (mAIM1: W303A L306A; mAIM2: W488A L491A) in TaABS3 abolished the TaATG8d-TaABS3 interaction but did not interfere the LE localization of TaABS3 (Fig. 6d, e, Supplementary Fig. 7e). Lastly, we generated Arabidopsis transgenic lines expressing *p35S:TaABS3* or

p35S:TaABS3$^{mAIM1+mAIM2}$. Upon C-deprivation, *p35S:TaABS3* lines, but not *p35S:TaABS3*$^{mAIM1+mAIM2}$ lines, showed accelerated senescence and excessive loss of total cellular proteins compared to the WT (Fig. 6f–h). These data and the high homology between TaATG8d and AtATG8s suggest that the ABS3-mediated senescence pathway is likely conserved among dicot and monocot plants and the ATG8-ABS3 interaction module represents a conserved senescence regulation paradigm in higher plants.

Discussion

Cellular proteostasis is a key determinant of senescence and longevity, and proteostasis dysfunction is often associated with premature senescence and diseases[1]. Protein degradation systems, including the canonical autophagy pathway, are expected to maintain cellular proteostasis[1]. In higher plants, defects in canonical autophagy leads to accelerated senescence under natural or stress conditions[35–38]. The counter-intuitive fact that cellular protein degradation is accelerated in plant *atg* mutants suggests the presence of additional senescence pathway(s). However, the nature of these pathway(s) remains poorly understood.

In this study, we discovered that six LE-localized *Arabidopsis* ABS3 subfamily MATE transporters act redundantly to promote natural and C-deprivation-induced senescence (Figs. 1 and 5). The hypersensitivity to C-deprivation of *ABS3* gain-of-function mutants is reminiscent of loss-of-function mutants in autophagy[2,3], suggesting the opposite consequences of two catabolic pathways. However, clear functional distinctions exist between ABS3-mediated pathway and autophagy, as *ABS3* gain-of-function mutants display additional developmental phenotypes that are not associated with plant autophagy mutants[27,30]. In-depth genetic dissection of ABS3-mediated pathway and autophagy pathway showed that the accelerated protein degradation and senescence phenotypes of *atg* mutants were suppressed by the higher-order *mate* mutants but further worsened in *abs3–1D* (Fig. 2). To our knowledge, *mateq* mutant represents the first known genetic condition that could circumvent autophagy deficiency to prevent senescence and promote plant longevity during C-deprivation. Our findings suggest that ABS3 subfamily MATE transporters are required for the senescence program under C-deprivation or canonical autophagy deficiency.

Furthermore, we discover that ABS3 subfamily MATEs interact with ATG8 at LE to promote senescence (Fig. 3). The C-terminal processing of ATG8, the subsequent conjugation of ATG8 to ATG8-PE, and the recruitment of ATG8-PE to autophagic membranes are conserved and obligatory steps in autophagy[3,15]. In contrast, ATG8-ABS3 interaction at LE does not require the formation of ATG8-PE or the ATG5/7-dependent canonical autophagy (Figs. 4f–i, 5e). Thus, our findings reveal a non-autophagic function of ATG8 in the ABS3-mediated senescence pathway. Importantly, this ABS3-mediated pathway is likely conserved in higher plants as we observed a similar TaATG8-TaABS3 function module in monocotyledonous wheat (Fig. 6). Although non-autophagic functions of ATG proteins have recently emerged[49,50], the discovery that ATG8-ABS3 interaction controls plant senescence is unprecedented. Given the membrane tethering ability of ATG8 and the potential large number of ATG8-interacting proteins in plants and animals[51,52], ATG8 and related proteins could act as central and versatile facilitators of cellular processes

beyond autophagy. The identification of ABS3 subfamily MATEs as novel ATG8 interactors expanded the known ATG8 interactome and cellular functions.

Based on our findings, we propose a model in which the ATG8-ABS3 pathway and the canonical autophagy act in parallel and control plant senescence and longevity (Fig. 7). Under mild nutrient limitation, autophagy is activated and utilizes ATG8 to promote plant longevity. However, under severe nutrient deprivation, or when autophagy is blocked, the previously unrecognized ATG8-ABS3 pathway promotes plant senescence (Fig. 7). Under C-deprivation, ATG8-ABS3 interaction promotes the ABS3 trafficking to vacuole lumen and its degradation in the vacuole (Fig. 5). The trafficking of ABS3 into vacuole is clearly independent of autophagy. Given the presence of ABS3 on LE, ABS3-GFP trafficking may be mediated by endosome vacuole fusion. However, how ABS3-GFP is delivered to vacuole lumen remains unclear, and additional mechanism might be involved[53]. Since ABS3-mediated senescence is neither alleviated nor enhanced by the increased amount of ATG8 protein (Fig. 5g), additional factors may be needed for the partitioning of ATG8s to the senescence-preventing autophagy pathway or the senescence-promoting ABS3 pathway. It is possible that interaction between ATG8-ABS3 interaction and the subsequent degradation of ABS3 in the vacuole triggers a retrograde signal that activates the senescence program in a nutrient-dependent manner. In this scenario, the flux of ABS3 to the vacuole may serve as a means for the vacuole to sense the nutrient status of the cell. Our findings uncover a new non-autophagic function of ATG8 and establish the noncanonical ATG8-ABS3 pathway as an evolutionarily conserved senescence regulatory mechanism in higher plants.

Methods

Plant materials and growth conditions

All Arabidopsis strains used in this study are of the Columbia-0 (Col-0) background. Arabidopsis mutants *atg5–1* (SAIL_129_B07)[37], *atg7–3* (SAIL_11_H07)[54], *abs3–1D*[30], *abs4–1D*[30], *abs3–1* (SM3_36823)[30], *abs4–1* (SALK_067667)[30], *abs3l1–1* (SAIL_1236_H10)[30], and *abs3l2–1* (SALK_144096)[30] have been described; *abs3l3–1* (SALK_127812) and *abs3l4–1* (SALK_128217) were obtained from the Arabidopsis Resource Center (ABRC). Quadruple mutant *mateq* (*abs3–1 abs4–1 abs3l1–1 abs3l2–1*) has been described[30]; higher order mutants *mated* (*abs3–1 abs4–1* double mutant), *mates* (*abs3–1 abs4–1 abs3l1–1 abs3l2–1 abs3l3–1 abs3l4–1* sextuple mutant), *abs3–1D atg7–3* double mutant, *mateq atg7–3* quintuple mutant, *abs3–1D atg5–1* double mutant, and *mateq atg5–1* quintuple mutant were generated in this study. Arabidopsis transgenic line expressing *pUBQ10:YFP-ARA7* (wave_2Y) has been described[55]. Primers used for genotyping were listed in Supplementary Table 1.

Plants for protoplast preparation were grown on Jiffy-7-Peat Pellets (Jiffy Group) and kept in a growth chamber set at 22°C, ~75 μmol m^{-2} s^{-1} illumination, 12 hr/12 hr day/night cycle. Plants for other purposes were grown on commercial soil mix (Pindstrup, Denmark), placed in a growth room kept at 22°C with continuous illumination of ~80 μmol m^{-2} s^{-1}.

C-deprivation treatment

Arabidopsis seeds were first surface sterilized with a solution containing 50% (v/v) bleach and 0.1% (v/v) Triton X-100 for 5 min and washed seven times with sterilized water. After 3-day stratification at 4°C, seeds were planted on 1/2 Murashige & Skoog (MS) basal salts mixture (M153, PhytoTechnology Laboratories) supplemented with 1% (w/v) sucrose and 1% (w/v) BactoAgar (214010, BD). 1/2 MS plates were then placed vertically in a growth chamber under continuous illumination of ~75 μmol m^{-2} s^{-1}. For C-deprivation treatment, 7-day-old seedlings were transferred to 1/2 MS plates without sucrose, wrapped in aluminum foil for dark treatment in the same growth chamber for indicated time periods. Seedlings immediately after transplantation served as 0d C-deprivation control.

N-starvation treatment

Arabidopsis seeds were sown on 1/2 MS basal salts mixture without nitrogen (M531, PhytoTechnology Laboratories) supplemented with 10 mM KNO_3, 1% (w/v) sucrose, and 1% (w/v) BactoAgar. 7-d-old seedlings were then transferred to the same medium with 10 mM KCl (N-starvation) or 10 mM KNO_3 (control treatment) for 4 days. Plants were kept under continuous light (~80 μmol m^{-2} s^{-1}) at 22°C before and during N-starvation.

Vector construction

Detailed information of primers used for vector construction were listed in Supplementary Table 1. A list of all the vectors used in this study is provided in Supplementary Table 2.

Briefly, for co-localization studies, coding sequences of fluorescent proteins GFP, mCherry and mScarlet[42] with or without the stop codon were amplified and placed in the *pUC18* backbone between the 35S promoter and NOS terminator. CDS of Arabidopsis *MATE* genes were fused at the N-terminal of GFP coding sequences to generate *pUC18-p35S:MATE-GFP*. CDS of *Arabidopsis ATG8* genes were fused at the C-terminal of GFP to generate *pUC18-p35S:GFP-ATG8*. *TaABS3* and *TaATG8d* mRNA sequences were obtained by performing blast searches using ABS3 and ATG8e protein sequences as queries, respectively. *TaABS3* and *TaATG8d* cDNA sequences were amplified from cDNAs synthesized from wheat seedlings, cloned into *pUC18-p35S:GFP* vector, and verified by sequencing. CDS of *ARA7* was fused at the C-terminal of mScarlet to generate *pUC18-p35S:mScarlet-ARA7*. CDS of *ABS3* was fused at the C-terminal of mCherry to generate *pUC18-p35S:mCherry-ABS3*. Vectors harboring mutated versions of *ABS3*, *TaABS3*, or Arabidopsis *ATG8e* were generated using the Q5 Site-Directed Mutagenesis Kit (E0554S, New England BioLabs). For the bimolecular fluorescence complementation (BiFC) assay, the expression cassettes for YN (N-terminal of eYFP) and YC (C-terminal of eYFP) together with the polylinker sequence were digested from *pSPYNE(R)173* and *pSPYCE(M)*[43], and cloned into pUC18 backbone to generate *pUC18-p35S:YN* and *pUC18-p35S:YC*, respectively. CDS of *MATE* genes were fused at C-terminal of YN to generate *pUC18-p35S:YN-MATE*. CDS of 9 Arabidopsis *ATG8* genes and wheat *TaATG8d* were fused at C-terminal of YC to generate *pUC18-p35S:YC-ATG8*. Vectors for the split-ubiquitin assay were constructed as described[44].

Generation of transgenic lines

For plant transformation, coding sequences for ABS3-GFP, ABS3^{P66A}, ABS3$^{mAIM1+mAIM2}$, ABS3$^{mAIM+mAIM2}$-GFP, TaABS3, TaABS3$^{mAIM+mAIM2}$, and ATG8e, were subcloned into a binary vector *pBI111L*[56] between the 35S promoter and the NOS terminator. *pBI111L-pABS3:ABS3-GFP* was generated by replacing the 35S promoter in *pBI111L* with *ABS3* endogenous promoter sequences[30]. The floral dip method was used for generating transgenic lines[57]. T1 plants were screened on solid 1/2 MS medium supplemented with 1% (w/v) sucrose, 1% (w/v) BactoAgar and 50 μg mL^{-1} kanamycin.

Protein and chlorophyll contents measurement

For measuring protein and chlorophyll contents from the same sample, whole seedlings were harvested from vertical plates, weighed, frozen, and ground in liquid nitrogen. Ground tissues were resuspended in 50 mM Tris-HCl pH 6.8, 2% SDS, 10% glycerol. 50 μl tissue resuspension from each sample were saved for chlorophyll measurement. The rest of the tissue resuspensions were incubated at 95°C for 5 min to extract protein. Supernatants were collected after spinning at 14,000 rpm at room temperature for 10 min. Protein contents in supernatants were measured using The Pierce™ BCA Protein Assay Kit (23227, ThermoFisher Scientific) following the manufacturer's manual. Chlorophyll were extracted by adding 450 μl 95% ethanol to 50 μl tissue resuspension and incubated at 4°C in the dark. Supernatants were separated from tissue debris by centrifugation at 14,000 rpm at 4°C for 10 min. Absorbance at 649 nm and 664 nm of the supernatant were measured. Chlorophyll content was calculated as described[58]. Protein and chlorophyll contents were normalized to equal amount of fresh tissue weight. Three biological replicates were included.

Immunoblot analysis

For SDS-PAGE and immunoblotting, seedlings were weighed, frozen, and ground in liquid nitrogen and incubated with the lysis buffer containing 0.125 M Tris-HCl pH 6.8, 4% SDS, 20% glycerol for 2 hours at 65°C. Samples were normalized by adjusting the lysis buffer volumes based on the fresh tissue weight. After incubation, total cell extracts were centrifuged at 14,000 rpm for 10 min at room temperature to remove the tissue debris.

To compare the total cellular protein levels in different samples and to separate ATG8 and ATG8-PE, a Urea-Tricine-SDS-PAGE system was utilized[59]. Proteins were then transferred onto a PVDF membrane and probed with a polyclonal ATG8 antibody prepared in house. ATG8 antibody was prepared as described[60]. To detect NBR1, RBCL, and PBA1, protein samples were separated by standard SDS-PAGE, transferred onto a nitrocellulose membrane, and probed with specific antibodies (anti-NBR1, AS142805, Agrisera; anti-RBCL AS03037, Agrisera; anti-PBA1, ab98861, Abcam).

RNA extraction and RT-qPCR

Total RNAs were prepared from seedlings using the Trizol RNA reagent (15596018, Thermo Fisher Scientific) following the manufacturer's manual. cDNA was synthesized from 1 μg total RNA using the Transcriptor First Strand cDNA Synthesis Kit (04897030001, Roche). qPCRs were performed using FastStart Essential DNA Green Master (06924204001, Roche) on a CFX96 Touch Real-Time PCR Detection System (Bio-Rad). Primers for qPCRs were

listed in Supplementary Table 1. Three or four biological replicates were included for data quantification. Expression of *ACT2* was used as an internal control.

Split-ubiquitin assay

Procedure for the split-ubiquitin assay has been described[44]. Briefly, to detect interaction between ATG8e and ABS3, *XN21 ATG8e-NubG* and *MetYC ABS3-CubPLV* were co-transformed into yeast strain THY.AP4. To detect interaction between ATG8e and ABS4, *NX33 NubG-ATG8e* and *MetYC ABS4-CubPLV* were co-transformed into yeast strain THY.AP4. Different NubG vectors were used to minimize the false positive interaction. Co-transformed yeast cells were selected on the SD-Leu-Trp medium. Single colonies were inoculated in liquid SD-Leu-Trp medium and 10-fold serial dilutions from saturated liquid cultures were spotted on SD-Leu-Trp-His-Ade +X-gal selection medium to detect protein interaction.

Protoplast transfection and spinning-disk confocal microscopy

Arabidopsis leaf protoplasts were prepared as described[61]. For co-transfections, 10 μg of each vector were used to transfect 200 μl protoplasts (2×10^5 ml^{-1}). After transfection, protoplasts were incubated for 10–12 hours before examined with a spinning-disk confocal system equipped with a CSU-W1 spinning-disk head (Yokogawa) and a iXon Ultra 888 EMCCD (Andor) on a DMi8 microscope body (Leica). Specifically, protoplasts were imaged with a HCX PL Apo 1.44 N.A. 100× oil immersion objective. GFP and YFP were excited at 488 nm. mCherry and mScarlet signals were excited at 561 nm. A TR-F525/50 or a TR-F593/46 bandpass emission filter (Semrock Brightline) was used for capturing GFP/YFP or mCherry/mScarlet signals. Confocal images were processed with the Fiji-ImageJ software[62]. To quantify BiFC assays, *p35S:mScarlet-ARA7* were co-transfected with BiFC vectors as a transfection control. Interactions of YN and YC fusion proteins were quantified as the percentage of cells with YFP signals of the total transfected cells (cells with mScarlet-ARA7 signals). Three independent sets of experiments were performed and quantified for each pair of YN and YC vectors. Note that BiFC quantification data summarized in Supplementary Fig. 5f was also shown in Figs. 4c, 4g-4i, and 5b as mean ± s.d.

Magic Red Cathepsin B Assay

Magic Red Cathepsin B staining was performed on protoplasts prepared from cotyledons of 7-d-old seedlings following the manufacturer's instructions (#937, ImmunoChemistry Technologies). After incubation, protoplasts were imaged by a fluorescence microscope (DMi8, Leica) equipped with a DFC 365FX CCD (Leica) using the 10× objective lens. Fluorescence intensities of each cell were measured by Fiji-ImageJ software.

GST pull-down assay

Recombinant GST, or GST-ATG8e proteins were produced by transforming *E. coli* strain BL21(DE3) with *pGEX 4T-1* (27–4580–01, GE Healthcare) or *pGEX 4T-1-ATG8e* and purified with Glutathione Sepharose 4B beads (17–0756–01, GE Healthcare) following the manufacturer's instructions. To pull-down ABS3-GFP from *p35S:ABS3-GFP* transgenic

lines, the membrane fraction was prepared from 0.5 g fresh tissue of *p35S:ABS3-GFP* plants as described[63] and incubated with 10 µl Glutathione Sepharose 4B beads loaded with 100 µg of purified GST or GST-ATG8e at 4°C overnight in pull-down buffer (100 mM Tris-HCI, pH 7.3, 150 mM NaCl, 1 mM EDTA, 1% Triton X-100, 10% Glycerol, 1× protease inhibitor cocktail [4693159001, Roche]). After incubations, beads were washed 5 times with washing buffer (100 mM Tris-HCI, pH 7.3, 150 mM NaCl, 1 mM EDTA, 1× protease inhibitor cocktail [4693159001, Roche]) and eluted by boiling in 2X SDS sample buffer. Presence of ABS3-GFP in the elutes was detected by immunoblotting using a monoclonal anti-GFP antibody (632381, Clontech).

E. coli mutant growth complementation assay

Growth complementation assay was carried out using the drug-sensitive *E. coli* strain (BW25113) *ΔacrB* as described in[45]. In brief, coding sequences for ABS3 or ABS3^{P66A} were cloned into *pMAL-c4X* (New England Biolabs) and the resulting vectors *pMAL-c4X-ABS3* and *pMAL-c4X-ABS3^{P66A}* were used to transform the *ΔacrB* strain. Transformants were steaked on LB plates containing 0.25 mM IPTG to induce the expression of *ABS3* or *ABS3^{P66A}*. Norfloxacin (0.02 µg ml^{-1}) (70458967, Sigma) was added to the plates to test drug resistance.

Drug treatment

To treat protoplasts with E-64d (sc-201280A, Santa Cruz Biotechnology), 20 µM E-64d or equal volume of DMSO (0.1%, v/v) was added to the protoplast incubation solution right after transfection. To treat seedlings with E-64d, 7-day-old seedlings grown on vertical plates were transferred to liquid 1/2 MS medium containing 20 µM E-64d or equal volume of DMSO (0.1%, v/v). To treat seedlings with wortmannin (S2758, Selleck), 4-day-old seedlings grown on vertical plates were transferred to liquid 1/2 MS medium containing 30 µM wortmannin or equal volume of DMSO (0.1%, v/v) for 1 hour before examining with the spinning-disk confocal microscopy.

Accession Numbers

Sequence data for genes used in this study can be found in The Arabidopsis Information Resource (TAIR) (www.arabidopsis.org) under the following accession numbers: ABS3, At4g29140; ABS4, At1g58340; ABS3L1, At5g19700; ABS3L2, At5g52050; ABS3L3, At4g23030; ABS3L4, At2g38510; ATG8a, At4g21980; ATG8b, At4g04620; ATG8c, At1g62040; ATG8d, At2g05630; ATG8e, At2g45170; ATG8f, At4g16520; ATG8g, At3g60640; ATG8h, At3g06420; ATG8i, At3g15580; ARA7, At4g19640.

Data Availability

The data that support the findings of this study are available from the corresponding author upon request.

Supplementary Material

Refer to Web version on PubMed Central for supplementary material.

Acknowledgements

This work was supported by grants from the National Natural Science Foundation of China (31570267 to F.Y., 31770205 to X.L., and 31741010 to Y.Q.) and Northwest A&F University (2452016001 to F.Y.). Y.W., L.S., and J.S. were supported by the US National Institute of Health grant R01GM06493. We thank the Teaching and Research Core Facility at College of Life Science, NWAFU for their support in this work. We thank members of the Sheen lab and Dr. Kai Mao of Massachusetts General Hospital and Harvard Medical School, USA for the stimulating discussions and critical reading of the manuscript.

References

1. Riera CE, Merkwirth C, De Magalhaes Filho CD & Dillin A Signaling networks determining life span. Annu. Rev. Biochem 85, 35–64 (2016). [PubMed: 27294438]
2. Li F & Vierstra RD Autophagy: a multifaceted intracellular system for bulk and selective recycling. Trends Plant Sci. 17, 526–537 (2012). [PubMed: 22694835]
3. Liu Y & Bassham DC Autophagy: pathways for self-eating in plant cells. Annu. Rev. Plant Biol. 63, 215–237 (2012). [PubMed: 22242963]
4. Xiong Y et al. Glucose-TOR signalling reprograms the transcriptome and activates meristems. Nature 496, 181–186 (2013). [PubMed: 23542588]
5. Sheen J Master regulators in plant glucose signaling networks. J. Plant Biol. 57, 67–79 (2014). [PubMed: 25530701]
6. Xiong Y & Sheen J Novel links in the plant TOR kinase signaling network. Curr. Opin. Plant Biol. 28, 83–91 (2015). [PubMed: 26476687]
7. Baena-González E, Rolland F, Thevelein JM & Sheen J A central integrator of transcription networks in plant stress and energy signalling. Nature 448, 938–942 (2007). [PubMed: 17671505]
8. Lim PO, Kim HJ & Nam HG Leaf senescence. Annu. Rev. Plant Biol. 58, 115–136 (2007). [PubMed: 17177638]
9. Thomas H Senescence, ageing and death of the whole plant. New Phytol. 197, 696–711 (2013). [PubMed: 23176101]
10. Woo HR, Kim HJ, Nam HG & Lim PO Plant leaf senescence and death - regulation by multiple layers of control and implications for aging in general. J. Cell Sci. 126, 4823–4833 (2013). [PubMed: 24144694]
11. Kim J, Woo HR & Nam HG Toward systems understanding of leaf senescence: an integrated multi-omics perspective on leaf senescence research. Mol. Plant 9, 813–825 (2016). [PubMed: 27174403]
12. Guo Y & Gan S-S Convergence and divergence in gene expression profiles induced by leaf senescence and 27 senescence-promoting hormonal, pathological and environmental stress treatments. Plant, Cell & Environ. 35, 644–655 (2012).
13. Liebsch D & Keech O Dark-induced leaf senescence: new insights into a complex light-dependent regulatory pathway. New Phytol. 212, 563–570 (2016). [PubMed: 27716940]
14. Kaur J & Debnath J Autophagy at the crossroads of catabolism and anabolism. Nat. Rev. Mol. Cell Biol. 16, 461–472 (2015). [PubMed: 26177004]
15. Xie Z & Klionsky DJ Autophagosome formation: core machinery and adaptations. Nat. Cell Biol. 9, 1102–1109 (2007). [PubMed: 17909521]
16. Michaeli S, Galili G, Genschik P, Fernie AR & Avin-Wittenberg T Autophagy in plants--What's new on the menu? Trends Plant Sci. 21, 134–144 (2016). [PubMed: 26598298]
17. Soto-Burgos J, Zhuang X, Jiang L & Bassham DC Dynamics of autophagosome formation. Plant Physiol. 176, 219–229 (2018). [PubMed: 29061903]
18. Morita Y, Kataoka A, Shiota S, Mizushima T & Tsuchiya T NorM of vibrio parahaemolyticus is an Na(+)-driven multidrug efflux pump. J. Bacteriol 182, 6694–6697 (2000). [PubMed: 11073914]
19. Ogawa T et al. Stimulating S-adenosyl-l-methionine synthesis extends lifespan via activation of AMPK. Proc. Natl. Acad. Sci. U.S.A. 113, 11913–11918 (2016). [PubMed: 27698120]
20. Otsuka M et al. A human transporter protein that mediates the final excretion step for toxic organic cations. Proc. Natl. Acad. Sci. U.S.A. 102, 17923–17928 (2005). [PubMed: 16330770]

21. Li L, He Z, Pandey GK, Tsuchiya T & Luan S Functional cloning and characterization of a plant efflux carrier for multidrug and heavy metal detoxification. J. Biol. Chem 277, 5360–5368 (2002). [PubMed: 11739388]
22. Diener AC, Gaxiola RA & Fink GR Arabidopsis ALF5, a multidrug efflux transporter gene family member, confers resistance to toxins. Plant Cell 13, 1625–1638 (2001). [PubMed: 11449055]
23. Rogers EE & Guerinot ML FRD3, a member of the multidrug and toxin efflux family, controls iron deficiency responses in Arabidopsis. Plant Cell 14, 1787–1799 (2002). [PubMed: 12172022]
24. Magalhaes JV et al. A gene in the multidrug and toxic compound extrusion (MATE) family confers aluminum tolerance in sorghum. Nat. Genet 39, 1156–1161 (2007). [PubMed: 17721535]
25. Marinova K et al. The Arabidopsis MATE transporter TT12 acts as a vacuolar flavonoid/H^+-antiporter active in proanthocyanidin-accumulating cells of the seed coat. Plant Cell 19, 2023–2038 (2007). [PubMed: 17601828]
26. Serrano M et al. Export of salicylic acid from the chloroplast requires the multidrug and toxin extrusion-like transporter EDS5. Plant Physiol. 162, 1815–1821 (2013). [PubMed: 23757404]
27. Li R et al. ADP1 affects plant architecture by regulating local auxin biosynthesis. PLoS Genet. 10, e1003954 (2014). [PubMed: 24391508]
28. Zhang H et al. A DTX/MATE-type transporter facilitates abscisic acid efflux and modulates ABA sensitivity and drought tolerance in Arabidopsis. Mol. Plant 7, 1522–1532 (2014). [PubMed: 24851876]
29. Tian W et al. A molecular pathway for CO_2 response in Arabidopsis guard cells. Nat. Commun 6, 6057 (2015). [PubMed: 25599916]
30. Wang R et al. A subgroup of MATE transporter genes regulates hypocotyl cell elongation in Arabidopsis. J. Exp. Bot 66, 6327–6343 (2015). [PubMed: 26160579]
31. Zhang H et al. Two tonoplast MATE proteins function as turgor-regulating chloride channels in Arabidopsis. Proc. Natl. Acad. Sci. U.S.A. 114, E2036–E2045 (2017). [PubMed: 28202726]
32. Dobritzsch M et al. MATE transporter-dependent export of hydroxycinnamic acid amides. Plant Cell 28, 583–596 (2016). [PubMed: 26744218]
33. Kim JH et al. Trifurcate feed-forward regulation of age-dependent cell death involving miR164 in Arabidopsis. Science 323, 1053–1057 (2009). [PubMed: 19229035]
34. Sato Y, Morita R, Nishimura M, Yamaguchi H & Kusaba M Mendel's green cotyledon gene encodes a positive regulator of the chlorophyll-degrading pathway. Proc. Natl. Acad. Sci. U.S.A. 104, 14169–14174 (2007). [PubMed: 17709752]
35. Hanaoka H et al. Leaf senescence and starvation-induced chlorosis are accelerated by the disruption of an Arabidopsis autophagy gene. Plant Physiol. 129, 1181–1193 (2002). [PubMed: 12114572]
36. Doelling JH, Walker JM, Friedman EM, Thompson AR & Vierstra RD The APG8/12-activating enzyme APG7 is required for proper nutrient recycling and senescence in Arabidopsis thaliana. J. Biol. Chem 277, 33105–33114 (2002). [PubMed: 12070171]
37. Thompson AR, Doelling JH, Suttangkakul A & Vierstra RD Autophagic nutrient recycling in Arabidopsis directed by the ATG8 and ATG12 conjugation pathways. Plant Physiol. 138, 2097–2110 (2005). [PubMed: 16040659]
38. Phillips AR, Suttangkakul A & Vierstra RD The ATG12-conjugating enzyme ATG10 is essential for autophagic vesicle formation in Arabidopsis thaliana. Genetics 178, 1339–1353 (2008). [PubMed: 18245858]
39. Svenning S, Lamark T, Krause K & Johansen T Plant NBR1 is a selective autophagy substrate and a functional hybrid of the mammalian autophagic adapters NBR1 and p62/SQSTM1. Autophagy 7, 993–1010 (2011). [PubMed: 21606687]
40. Cui Y et al. Biogenesis of Plant Prevacuolar Multivesicular Bodies. Mol. Plant 9, 774–786 (2016). [PubMed: 26836198]
41. Lee G-J, Sohn EJ, Lee MH & Hwang I The Arabidopsis rab5 homologs rha1 and ara7 localize to the prevacuolar compartment. Plant Cell Physiol. 45, 1211–1220 (2004). [PubMed: 15509844]
42. Bindels DS et al. mScarlet: a bright monomeric red fluorescent protein for cellular imaging. Nat. Methods 14, 53–56 (2017). [PubMed: 27869816]

43. Waadt R et al. Multicolor bimolecular fluorescence complementation reveals simultaneous formation of alternative CBL/CIPK complexes in planta. Plant J. 56, 505–516 (2008). [PubMed: 18643980]
44. Bashline L & Gu Y Using the split-ubiquitin yeast two-hybrid system to test protein-protein interactions of transmembrane proteins. Methods Mol. Biol 1242, 143–158 (2015). [PubMed: 25408451]
45. Tanaka Y et al. Structural basis for the drug extrusion mechanism by a MATE multidrug transporter. Nature 496, 247–251 (2013). [PubMed: 23535598]
46. Miyauchi H et al. Structural basis for xenobiotic extrusion by eukaryotic MATE transporter. Nat. Commun 8, 1633 (2017). [PubMed: 29158478]
47. Birgisdottir ÅB, Lamark T & Johansen T The LIR motif - crucial for selective autophagy. J. Cell Sci. 126, 3237–3247 (2013). [PubMed: 23908376]
48. Jacomin A-C, Samavedam S, Charles H & Nezis IP iLIR@viral: A web resource for LIR motif-containing proteins in viruses. Autophagy 13, 1782–1789 (2017). [PubMed: 28806134]
49. Subramani S & Malhotra V Non-autophagic roles of autophagy-related proteins. EMBO Rep. 14, 143–151 (2013). [PubMed: 23337627]
50. Schaaf MBE, Keulers TG, Vooijs MA & Rouschop KMA LC3/GABARAP family proteins: autophagy-(un)related functions. FASEB J. 30, 3961–3978 (2016). [PubMed: 27601442]
51. Kriegenburg F, Ungermann C & Reggiori F Coordination of autophagosome-lysosome fusion by ATG8 family members. Curr. Biol 28, R512–R518 (2018). [PubMed: 29689234]
52. Wild P, McEwan DG & Dikic I The LC3 interactome at a glance. J. Cell Sci. 127, 3–9 (2014). [PubMed: 24345374]
53. Cullen PJ & Steinberg F To degrade or not to degrade: mechanisms and significance of endocytic recycling. Nat. Rev. Mol. Cell Biol. 19, 679–696 (2018). [PubMed: 30194414]
54. Lai Z, Wang F, Zheng Z, Fan B & Chen Z A critical role of autophagy in plant resistance to necrotrophic fungal pathogens. Plant J. 66, 953–968 (2011). [PubMed: 21395886]
55. Geldner N et al. Rapid, combinatorial analysis of membrane compartments in intact plants with a multicolor marker set. Plant J. 59, 169–178 (2009). [PubMed: 19309456]
56. Yu F, Park S & Rodermel SR The Arabidopsis FtsH metalloprotease gene family: interchangeability of subunits in chloroplast oligomeric complexes. Plant J. 37, 864–876 (2004). [PubMed: 14996218]
57. Clough SJ & Bent AF Floral dip: a simplified method for Agrobacterium-mediated transformation of Arabidopsis thaliana. Plant J. 16, 735–743 (1998). [PubMed: 10069079]
58. Lichtenthaler HK [34] Chlorophylls and carotenoids: Pigments of photosynthetic biomembranes. in Plant Cell Membranes 350–382 (Elsevier, 1987). doi:10.1016/0076-6879(87)48036-1
59. Schägger H & von Jagow G Tricine-sodium dodecyl sulfate-polyacrylamide gel electrophoresis for the separation of proteins in the range from 1 to 100 kDa. Anal. Biochem 166, 368–379 (1987). [PubMed: 2449095]
60. Zhuang X et al. A BAR-domain protein SH3P2, which binds to phosphatidylinositol 3-phosphate and ATG8, regulates autophagosome formation in Arabidopsis. Plant Cell 25, 4596–4615 (2013). [PubMed: 24249832]
61. Yoo S-D, Cho Y-H & Sheen J Arabidopsis mesophyll protoplasts: a versatile cell system for transient gene expression analysis. Nat. Protoc 2, 1565–1572 (2007). [PubMed: 17585298]
62. Schindelin J et al. Fiji: an open-source platform for biological-image analysis. Nat. Methods 9, 676–682 (2012). [PubMed: 22743772]
63. Avila JR, Lee JS & Torii KU Co-immunoprecipitation of membrane-bound receptors. Arabidopsis Book 13, e0180 (2015). [PubMed: 26097438]

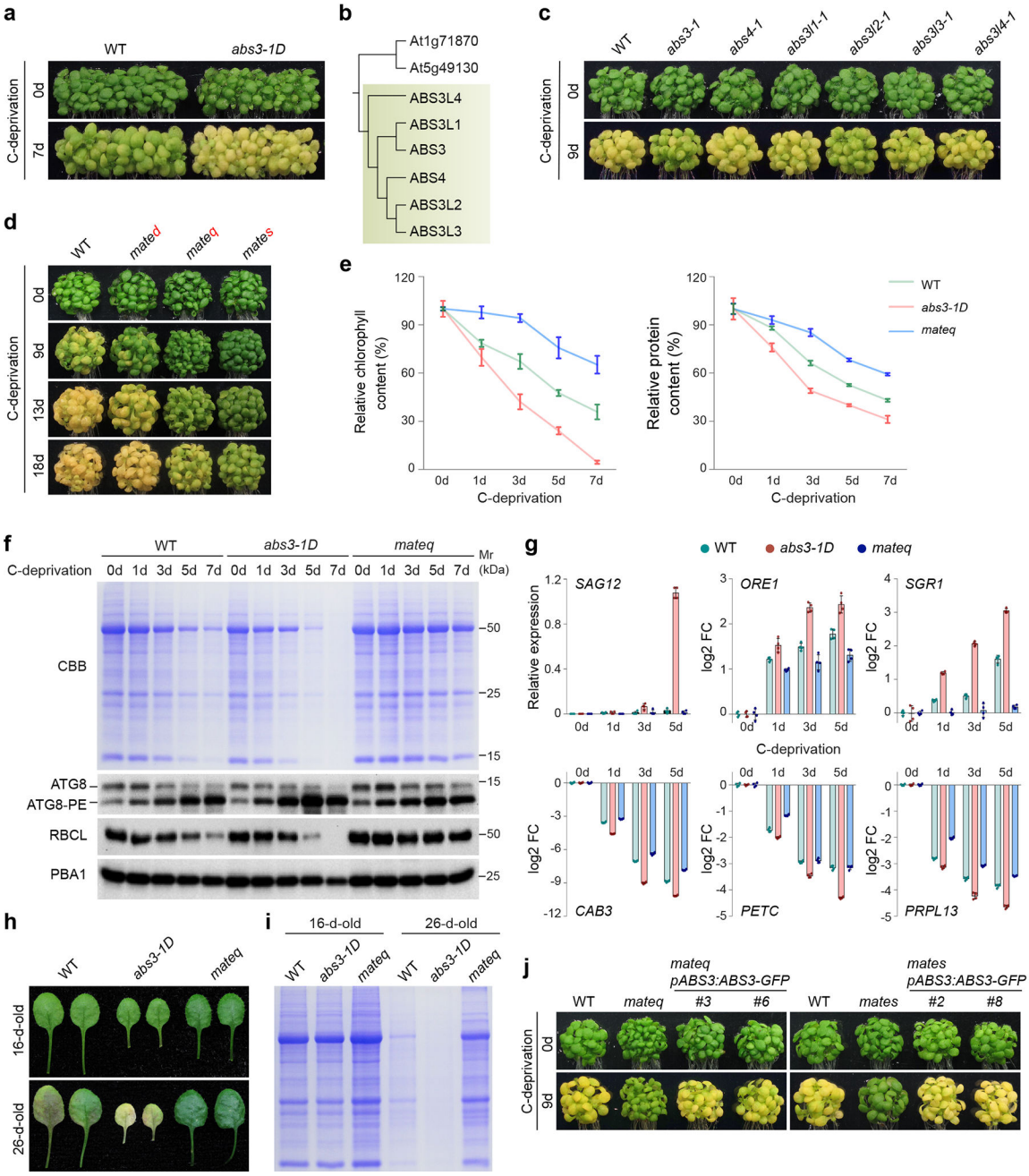

Fig. 1. ABS3 subfamily MATEs promote plant senescence.

a, Senescence phenotypes of wild type (WT) and *abs3–1D* before and after 7d C-deprivation. **b,** The phylogenetic clade consists of ABS3 subfamily MATE proteins (shaded part). **c,** Senescence phenotype of WT and single mutant of *ABS3* subfamily *MATE* genes before and after 9d C-deprivation. **d,** Senescence phenotype of WT, double mutant *mated* (*abs3–1 abs4–1*), quadruple mutant *mateq* (*abs3–1 abs4–1 abs3l1–1 abs3l2–1*), and sextuple mutant *mates* (*abs3–1 abs4–1 abs3l1–1 abs3l2–1 abs3l3–1 abs3l4–1*) before and after 9d, 13d, and 18d C-deprivation. **e,** Chlorophyll content and protein content (normalized to equal amounts of fresh weight) reduction in WT, *abs3–1D*, and *mateq* during C-deprivation. Data

were presented as mean ± standard deviation (s.d.) (n=3 biological replicates). **f,** Total cellular proteins from WT, *abs3–1D*, and *mateq* during C-deprivation were resolved on SDS-PAGE, stained by CBB or probed with indicated antibodies. anti-PBA1 served as a loading control. **g,** RT-qPCR analyses of indicated genes in WT, *abs3–1D*, and *mateq* during C-deprivation. Relative expression was shown for *SAG12*. The log2 FC (fold change) with respect to expression levels in the WT at 0d was shown for other genes. Data were presented as mean ± s.d. (n=4 biological replicates). **h,** First pairs of true leaves from 16-day-old and 26-day-old WT, *abs3–1D*, and *mateq*. **i,** Total cellular proteins in leaves shown in **h** were resolved on SDS-PAGE and stained by CBB. **j,** Complementation of *mateq* and *mates* by the expression of *pABS3:ABS3-GFP*. Experiments in **a**, **c**, **d**, **f**, **h**, **i**, and **j** were independently repeated three times with similar results.

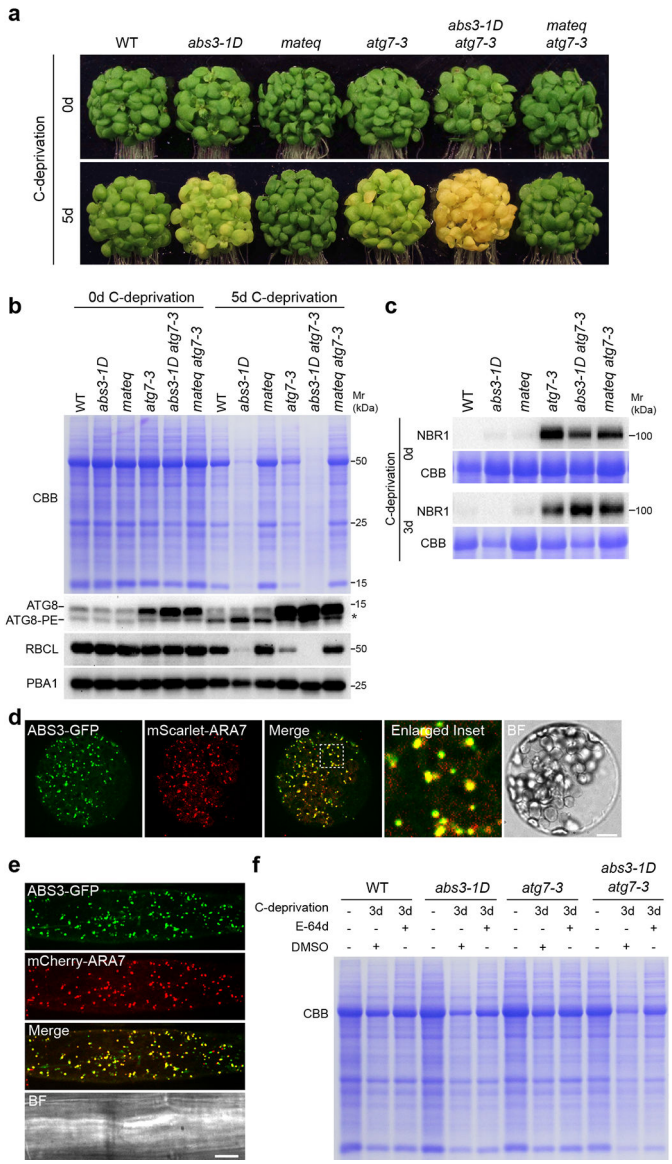

Fig. 2. Genetic interaction between *abs3–1D*, *mateq*, and autophagy mutant *atg7–3*.

a, Senescence phenotypes of WT, *abs3–1D*, *mateq*, *atg7–3*, *abs3–1D atg7–3* double mutant, and *mateq atg7–3* quintuple mutant before and after 5d C-deprivation. **b,** Total cellular proteins from plants of indicated genotypes before and after 5d C-deprivation were resolved on SDS-PAGE, probed with indicated antibodies or stained by CBB. Asterisk indicates a distinct ATG8 precursor or modification found in autophagy deficiency backgrounds. **c,** Immunoblot analysis of NBR1 accumulation in plants of indicated genotypes before and after 3d C-deprivation. **d,** Co-localization of ABS3-GFP and LE marker mScarlet-ARA7 in Arabidopsis leaf protoplasts. BF, bright field. Bar, 10 μm. **e,** Root epidermal cells of Arabidopsis transgenic line expressing both ABS3-GFP and mCherry-ARA7. Bars, 10 μm. **f,** Effects of E-64d on bulk protein reduction in WT, *abs3–1D*, *atg7–3*, and *abs3–1D atg7–3* after 3d C-deprivation. Experiments in **a**-**f** were independently repeated three times with similar results.

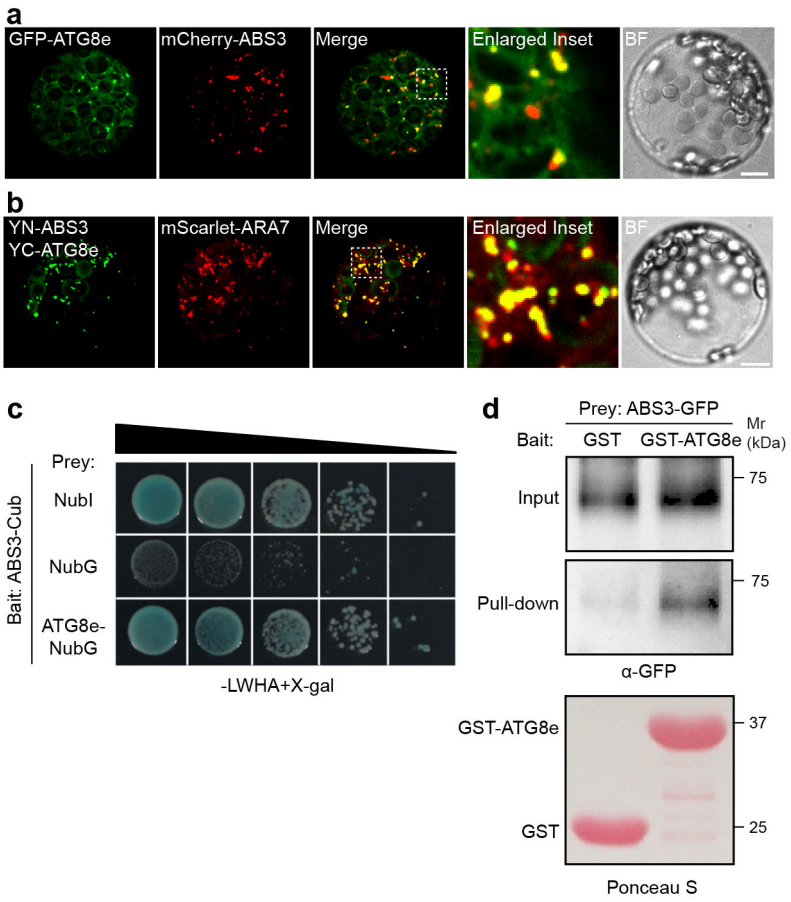

Fig. 3. Physical interaction between ABS3 and ATG8e.

a, Partial co-localization of GFP-ATG8e and mCherry-ABS3 in Arabidopsis leaf protoplasts. **b,** Protoplasts co-expressing YN-ABS3, YC-ATG8e, and mScarlet-ARA7. YN or YC, N or C-terminal of YFP. Bar, 10 μm. **c,** Interaction between ABS3 and ATG8e in split-ubiquitin assay. Cub, C-terminal half of ubiquitin; NubI, N-terminal half of native ubiquitin, positive control; NubG, N-terminal half of ubiquitin harboring I13G mutation, negative control. Illustrated was the growth of yeast colonies on selection medium. **d,** GST pull-down assay with membrane fractions from *p35S:ABS3-GFP* transgenic lines. Experiments in **a-d** were independently repeated three times with similar results.

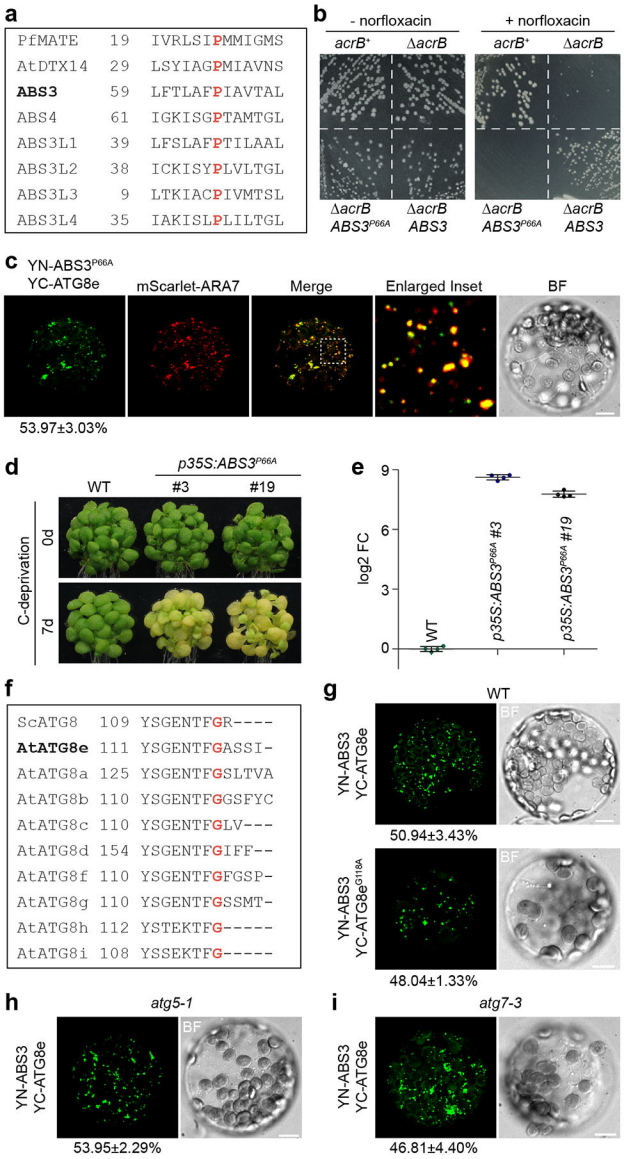

Fig. 4. ATG8-ABS3 interaction is independent of ABS3 transporter activity or ATG8-PE conjugation.

a, Conserved proline residue in PfMATE, AtDTX14, and ABS3 subfamily MATEs. **b,** Growth complementation assays of *E. coli ΔacrB* mutant expressing *ABS3* or *ABS3*^{P66A} on medium supplemented with antibiotic norfloxacin. **c,** Protoplasts co-expressing YN-ABS3^{P66A}, YC-ATG8e, and mScarlet-ARA7. Bars, 10 μm. **d,** Senescence phenotype of WT and two independent lines expressing *p35S:ABS3*^{P66A} before and after 7d C-deprivation. Experiments in **b** and **d** were independently repeated three times with similar results. **e,** RT-qPCR analysis of *ABS3* transcript levels in plants of indicated genotypes. The log2 FC was calculated with respect to the expression levels in the WT. Data were presented as mean ± s.d. (n=4 biological replicates). **f,** Conserved glycine residue in yeast (*S. cerevisiae*) and Arabidopsis ATG8s. **g,** BiFC assays comparing the interaction between YN-ABS3 and YC-ATG8e and the interaction between YN-ABS3 and YC-ATG8e^{G118A} in WT leaf protoplasts. **h, i,** BiFC assays detecting the interaction between YN-ABS3 and YC-ATG8e in *atg5–1* (**h**)

and *atg7–3* (**i**) protoplasts. Bars, 10 μm. Quantifications of BiFC assays in **c**, **g**, **h**, and **i** were carried out by co-transfecting protoplasts with BiFC vectors and *p35S:mScarlet-ARA7* as the transfection control. Percentages of cells showing YFP signals over the total number of cells expressing mScarlet-ARA7 were calculated. Data were shown as mean ± s.d. of three sets of experiments. See Supplementary Fig. 5 for the mScarlet-ARA7 panels of the same cells shown in **g**, **h**, and **i** and the statistical analysis.

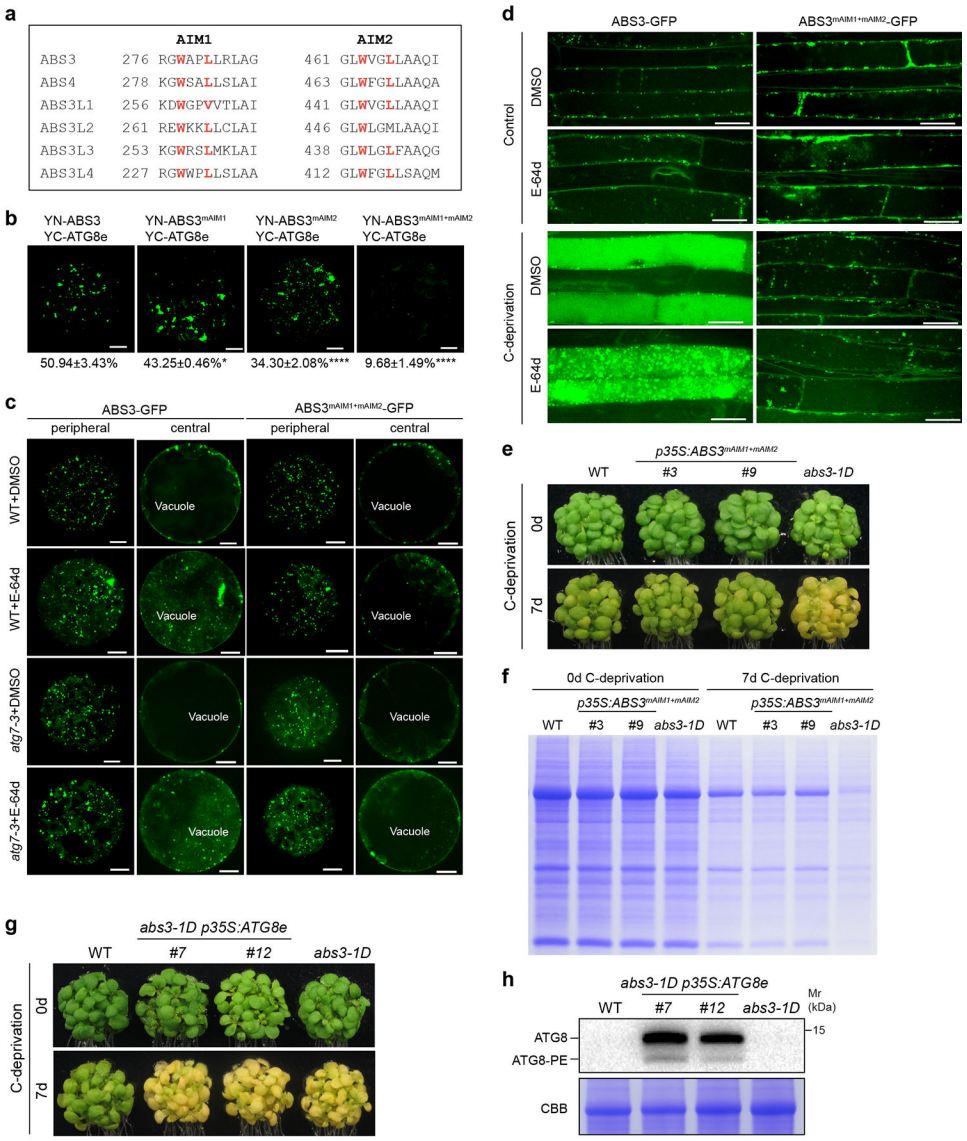

Fig. 5. ABS3-mediated senescence requires ATG8-ABS3 interaction.

a, Two conserved AIMs in ABS3 subfamily MATEs. **b,** BiFC assays to assess the interaction of YN-ABS3, YN-ABS3^{mAIM1}, YN-ABS3^{mAIM2}, or YN-ABS3$^{mAIM1+mAIM2}$ with YC-ATG8e in Arabidopsis leaf protoplasts. Bars, 10 μm. Quantifications of BiFC assays were shown as mean ± s.d. of three independent sets of experiments. *p=0.0125, ****p=0.0001, one-way ANOVA followed by Dunnett's multiple comparisons test. **c,** Subcellular distribution of transiently expressed ABS3-GFP and ABS3$^{mAIM1+mAIM2}$-GFP in WT and *atg7–3* protoplasts treated with DMSO or E-64d. Illustrated were images of the same protoplast focused to the periphery or to the center of the cell. Bars, 10 μm. **d,** Root epidermal cells of Arabidopsis transgenic lines expressing ABS3-GFP or ABS3$^{mAIM1+mAIM2}$-GFP. C-deprivation treatment was carried out by transferring 4-day-old seedlings to liquid medium without sucrose and placed in the dark for 12 hrs. Control plants were transferred to liquid medium with 1% sucrose and kept under light. Distribution patterns of ABS3-GFP or ABS3$^{mAIM1+mAIM2}$-GFP signals in the presence or absence of

E-64d were examined. Bars, 20 μm. **e,** Senescence phenotype of WT, two independent lines expressing *p35S:ABS3*$^{mAIM1+mAIM2}$, and *abs3–1D* before and after 7d C-deprivation. **f,** Total cellular proteins from plants of indicated genotypes before and after 7d C-deprivation were resolved on SDS-PAGE and stained by CBB. **g,** Senescence phenotype of WT, two independent lines expressing *p35S:ATG8e* in *abs3–1D* background, and *abs3–1D* before and after 7d C-deprivation. **h,** Immunoblot analysis of ATG8 and ATG8-PE accumulation in plants of indicated genotypes. Analyzed were total leaf proteins from 3-week-old plants. Experiments in **c**-**h** were independently repeated three times with similar results.

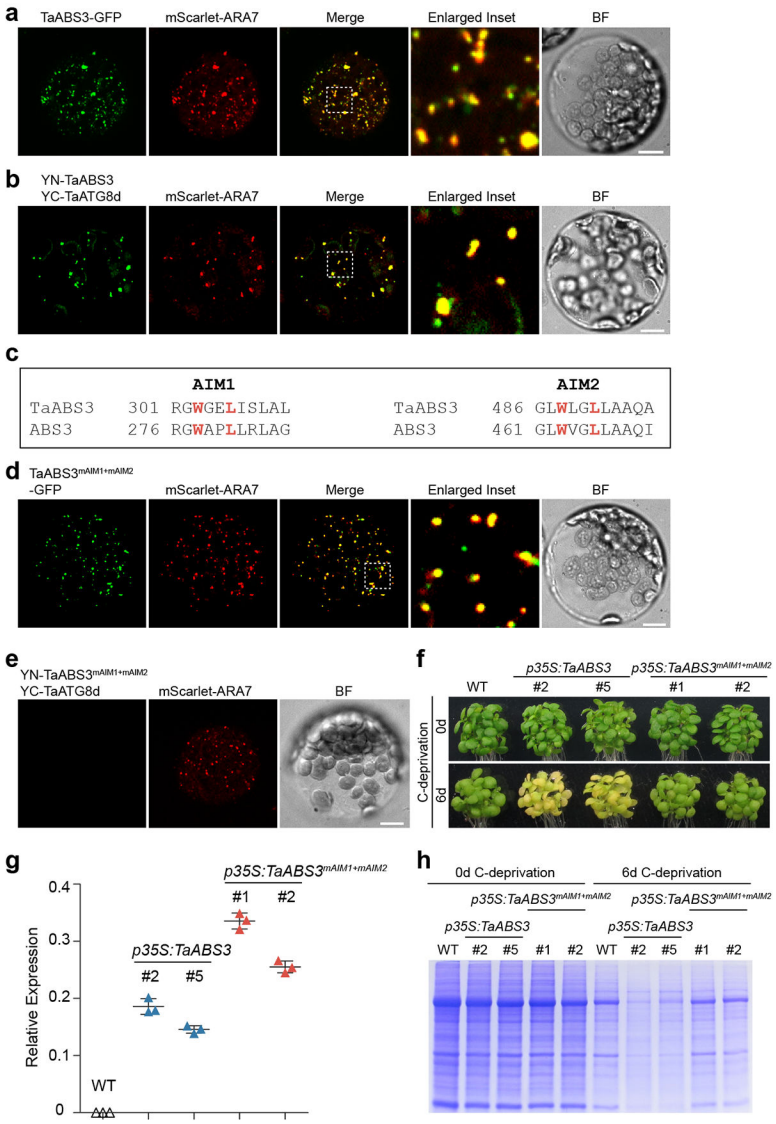

Fig. 6. Conserved ATG8-ABS3 interactions in wheat.

a, Co-localization of TaABS3-GFP and mScarlet-ARA7 in Arabidopsis leaf protoplasts. **b,** Protoplasts co-expressing YN-TaABS3, YC-TaATG8d, and mScarlet-ARA7. **c,** Two conserved AIMs in TaABS3. **d,** Co-localization of TaABS3$^{mAIM1+mAIM2}$-GFP and mScarlet-ARA7 in Arabidopsis protoplast. **e,** Protoplasts co-expressing YN-TaABS3$^{mAIM1+mAIM2}$, YC-TaTAG8d, and mScarlet-ARA7. Bars in **a**, **b**, **d** and **e,** 10 μm. **f,** Senescence phenotype of WT, two independent lines expressing *p35S:TaABS3*, and two independent lines expressing *p35S:TaABS3*$^{mAIM1+mAIM2}$ before and after 6d C-deprivation. **g,** RT-qPCR analysis of *TaABS3* transcripts levels in plants of indicated genotypes. Relative expressions of *TaABS3* were normalized to *ACT2*. Data were presented as mean ± s.d. (n=3 biological replicates). **h,** Total cellular proteins from plants of indicated genotypes before and after 6d C-deprivation were resolved on SDS-PAGE and stained by CBB. Experiments in **a**, **b**, **d**, **e**, **f**, and **h** were independently repeated three times with similar results.

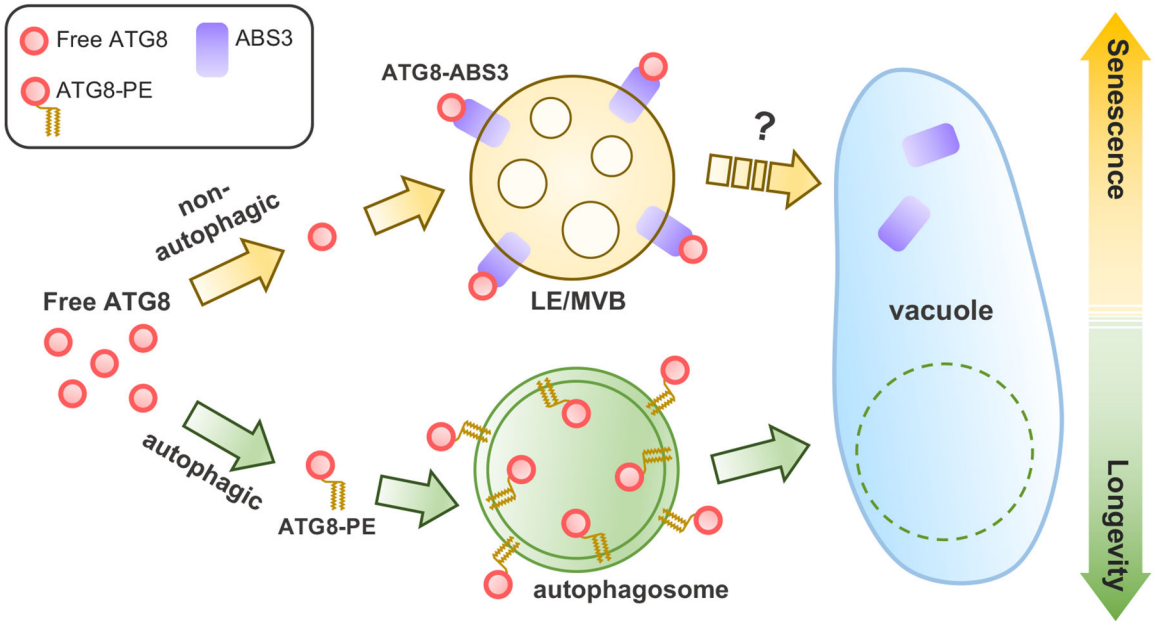

Fig. 7. Model for the ATG8-ABS3 interaction in controlling senescence in plants.
See "Discussion" for a detailed explanation of the model.